



Numerical simulation of high pressure gas quenching of H13 steel

Jing Wang^a, Jianfeng Gu^{a,*}, Xuexiong Shan^b, Xiaowei Hao^a, Nailu Chen^a, Weimin Zhang^a

^a Shanghai Key Laboratory of Materials Laser Processing and Modification, School of Materials Science and Engineering, Shanghai Jiao Tong University, Shanghai 200240, China

^b School of Naval Architecture, Ocean and Civil Engineering, Shanghai Jiao Tong University, Shanghai 200240, China

ARTICLE INFO

Article history:

Received 21 January 2006

Received in revised form

5 February 2007

Accepted 15 August 2007

Keywords:

Numerical simulation

Computational fluid dynamics

H13 steel

Gas quenching

ABSTRACT

Aided by the computational fluid dynamics software package FLUENT flow and heat-transfer model has been established to simulate the high pressure gas quenching process of a large H13 die. The complicate geometry mesh of finite volume method (FVM) simulation was exactly built according to the practical chamber set-up of vacuum furnace. The velocity and temperature distribution of gas, as well as the temperature field in H13 die, were obtained by simulation. The validation of simulation results has been carried out by comparing the simulated cooling curves of certain points inside the die with the measured ones. It can be found that the temperature depended thermal physical properties of gas and H13 die, such as thermal conductivity, specific heat and viscosity, have dramatic effects on the accuracy of simulation results. The possible improvement of the numerical simulation based on the detailed discussion is also elucidated.

© 2007 Elsevier B.V. All rights reserved.

1. Introduction

High pressure gas quenching is a form of heat treatment process used frequently in various industries and mostly for hardening of tool and die steels. The use of gas quenching can significantly improve the mechanical and physical properties of a material for obtaining near shape of metal components (Elkatatny et al., 2003). However, the cooling rate of gas quenching is lower than that of oil or water quenching, which limits the species and size of metal components. It is well known that the cooling efficiency of the gas quenching is influenced by the type of quench gas used (Stratton, 2002), the pressure, the velocity, the design factors relating to the size and shape of the chamber where quenching is taking place (Carter, 1996), and the load factors such as the material,

shape, weight and distribution of the load (Lubben et al., 2000). These factors are very important to in design of gas quenching technique, and it is almost impossible to find their rules by enormous experiment.

With the recent advances in computing power and memory, computational fluid dynamics (CFD) has become an important tool for the investigation of flow and heat-transfer problems (Lior, 2004). It has many advantages over the traditional approach of practical experimentation. For example, it permits the study of the effect of an individual factor without altering other variables; it can minimize the costs that would be required for equipment modifications and furnace's working time. Furthermore, potentially dangerous situations, such as those associated with extreme pressure or explosive gases, can be modeled safely (Pritchard et al., 1996).

* Corresponding author at: School of Materials Science and Engineering, Shanghai Jiao Tong University, Dongchuan Road 800, Shanghai 200240, China. Tel.: +86 21 34203743; fax: +86 21 34203742.

E-mail address: gujf@sjtu.edu.cn (J. Gu).

0924-0136/\$ – see front matter © 2007 Elsevier B.V. All rights reserved.

doi:10.1016/j.jmatprotec.2007.08.059

Although gas quenching process simulation with CFD has been realized for a long time, the results are far from satisfying, and have considerable discrepancy with experimental datum. In recent work by Elkatatny and Lior (Elkatatny et al., 2003; Lior, 2004), they simplified the vacuum chamber into a cubical block to make geometry model, and the components inside are neglected in simulation. Though helpful for meshing and convergence, these simplification and approximation also unavoidably bring about errors. In this work, CFD simulation of gas quenching has been carried out based on a complicate three dimensional geometry model according to the practical set-up of vacuum chamber.

2. Experimental

The vacuum gas quenching furnace used was manufactured by Shenyang Jiayu Vacuum Technology Co. Ltd. with the model of VHQ-446HF. The schematic diagram of one half of the symmetric quenching chamber is shown as Fig. 1. It can be seen that gas enters the chamber from circumferential nozzles and the hot gas leaves the heating chamber through outlet. The gas is recycled in a continuous gas quenching process when the hot gas flows through the heat exchanger and cools down. A die made of H13 hot work tool steel, with the dimension of 230 mm × 250 mm × 370 mm, was designed for simulation and quenching experiment. Five holes with the diameter of 3.2 mm were drilled, through which the thermocouples were fixed at the end of these holes by brazing inside the die (see Fig. 2). The cooling curves on these specific points during gas quenching were measured, and were simultaneously extracted from simulation results.

3. Formulation of numerical analysis

The fluid flow and temperature field of the load (H13 die) were modeled in three dimensions with the FLUENT computational

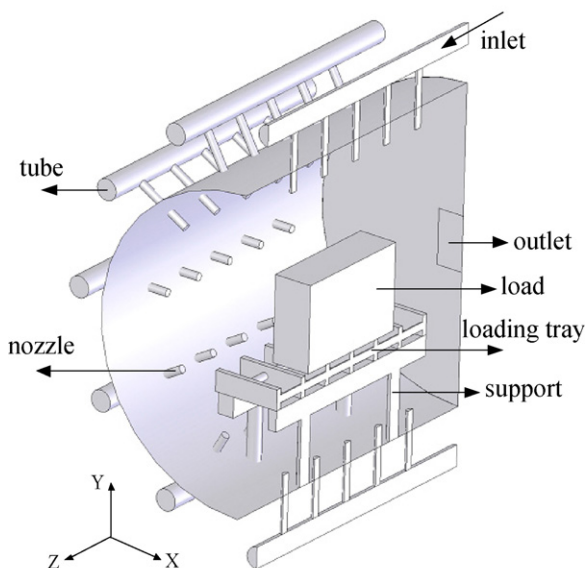


Fig. 1 – Set-up of gas quenching chamber used in the simulation.

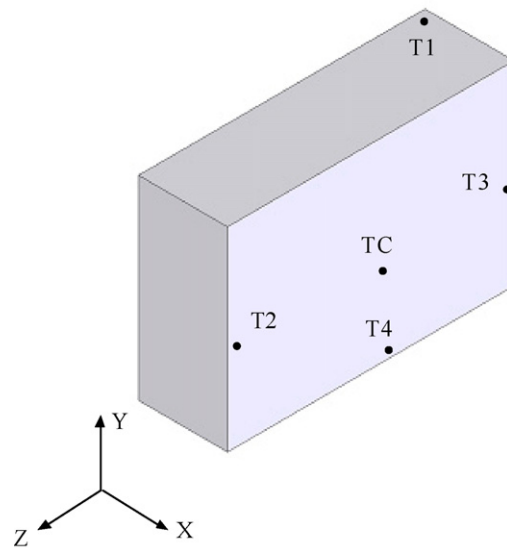


Fig. 2 – Schematic diagram showing the location of points in the die on which the cooling curves are measured.

fluid dynamics software package. In order to reduce the computational time, the numerical geometry model was made based on one-half of the real chamber as shown in Fig. 1, and more than two hundred ninety thousand cells were used to describe the chamber including the loading tray, the supports and the load. The numerical analysis has been performed on control volume approach, and all equations were solved using the second-order upwind discretization for convection and SIMPLE algorithm.

3.1. Transport equations

The basic mathematical equations for gas flow and heat transfer used can be described as follows (Fluent, 2002).

Continuity equation

$$\frac{\partial \rho}{\partial t} + \nabla \cdot (\rho U) = 0 \tag{1}$$

where ρ and U are the fluid density and velocity, respectively, t is the time.

Momentum equation

$$\frac{\partial \rho U}{\partial t} + \nabla \cdot (\rho U \otimes U) = -\nabla p + \nabla \cdot (\bar{\bar{T}}) + B \tag{2}$$

where p is the pressure, B is the body force, I is the unit tensor, μ is the molecular viscosity, and $\bar{\bar{T}}$ is the stress tensor by:

$$\bar{\bar{T}} = \mu \left[(\nabla U + (\nabla U)^T) - \frac{2}{3} \nabla U I \right] \tag{3}$$

Energy equation

For the fluid (gas)

$$\frac{\partial \rho H}{\partial t} + \nabla \cdot (\rho U H) - \nabla \cdot (\lambda \nabla T) = S_h \quad (4)$$

For the solid (die)

$$\frac{\partial \rho H}{\partial t} - \nabla \cdot (\lambda \nabla T) = S_h \quad (5)$$

where H is the total enthalpy: $H = c_p T$, c_p is specific heat, T is the temperature, λ is the thermal conductivity, S_h represents source term.

3.1.1. k - ε turbulent modeling

Forced, turbulent flow model was employed in the simulation, which is extremely complex time-dependent flow. It is not feasible to solve these equations with a reasonable accuracy using current technology for most problems. Reynolds average is usually adopted, in which the variables are split into their mean and fluctuating parts:

$$\Phi = \bar{\Phi} + \phi \quad (6)$$

Applying it to the basic Eqs. (1), (2) and (4), we can obtain:

$$\frac{\partial \rho}{\partial t} + \nabla \cdot (\rho U) = 0 \quad (7)$$

$$\frac{\partial \rho U}{\partial t} + \nabla \cdot (\rho U \times U) = -\nabla p + \nabla \cdot \left(\bar{T} - \rho \bar{\mathbf{u}} \times \bar{\mathbf{u}} \right) + B \quad (8)$$

$$\frac{\partial \rho T}{\partial t} + \nabla \cdot (\rho U T) - \nabla \cdot \left(\frac{\lambda}{c_p} \nabla T - \rho \bar{\mathbf{u}} T \right) = S_h \quad (9)$$

Here, U and T are mean part of the velocity and temperature, and \mathbf{u} is fluctuating part of velocity. Additional two terms, Reynolds stresses, $-\rho \bar{\mathbf{u}} \times \bar{\mathbf{u}}$, and Reynolds flux, $-\rho \bar{\mathbf{u}} T$, now appear, which represent the effects of turbulence. They must be pre-calculated in order to close Eqs. (8) and (9). A common method employs the Boussinesq hypothesis to relate the Reynolds stresses to the mean velocity gradients:

$$-\rho \bar{\mathbf{u}} \times \bar{\mathbf{u}} = \mu_t (\nabla U + (\nabla U)^T) + \frac{2}{3} (\rho k + \nabla U) I \quad (10)$$

and

$$-\rho \bar{\mathbf{u}} T = \frac{\mu_t}{Pr_t} \nabla T \quad (11)$$

where μ_t is turbulent viscosity, k is turbulence kinetic energy, Pr_t is the turbulent Prandtl number for energy and considered as a constant in Table 1. In order to solve μ_t , there are many turbulent models. In the case of the k - ε model, two additional transport equations (for the turbulence kinetic energy, k , and

the turbulence dissipation rate, ε) are introduced, and μ_t is computed as a function of k and ε as follow:

$$\mu_t = \rho C_\mu \frac{k^2}{\varepsilon} \quad (12)$$

where C_μ is a model constant and its value is given in Table 1.

The turbulence kinetic energy k and its rate of dissipation ε can be obtained from the following equations:

$$\frac{\partial \rho k}{\partial t} + \nabla \cdot (\rho U k) = \nabla \cdot \left(\left(\mu + \frac{\mu_t}{\sigma_k} \right) \nabla k \right) + G_k + G_b - \rho \varepsilon \quad (13)$$

$$\begin{aligned} \frac{\partial \rho \varepsilon}{\partial t} + \nabla \cdot (\rho U \varepsilon) = \nabla \cdot \left(\left(\mu + \frac{\mu_t}{\sigma_\varepsilon} \right) \nabla \varepsilon \right) \\ + C_1 \frac{\varepsilon}{k} (G_k + C_3 G_b) - C_2 \rho \frac{\varepsilon^2}{k} \end{aligned} \quad (14)$$

where σ_k and σ_ε are constants and given in Table 1. G_k represents the generation of turbulence kinetic energy due to the mean velocity gradients, can be calculated as:

$$G_k = \mu_t \nabla U \cdot (\nabla U + (\nabla U)^T) - \frac{2}{3} \nabla \cdot U (\mu_t \nabla \cdot U + \rho k) \quad (15)$$

G_b is the generation of turbulence kinetic energy due to buoyancy, can be calculated as:

$$G_b = -\frac{\mu_t}{\rho Pr_t} \mathbf{g} \cdot \nabla \rho \quad (16)$$

where \mathbf{g} is the gravitational vector. C_1, C_2, C_3 are constants and also given in Table 1.

3.2. Boundary and initial conditions

It is assumed that there is a constant gas velocity enters the chamber through every tube. The gas temperature changes with the cooling time according to the experimental data. The gas is nitrogen and the pressure is 2 bar. At the walls on the domain boundary adjacent to fluid cells, the velocity, the heat flux, and the flux of other transported scalars (e.g., mass fractions, volume fractions, etc.) are considered to be zero. The load, the loading tray and the supports are considered to be conduction solid with thermal physical properties of H13, Cr25Ni20Si2 and graphite, respectively. The initial the temperature field are set uniformly as 1050 °C.

3.3. Material properties

In simulation, the density of nitrogen is considered as a constant, and its thermal conductivity, specific heat and viscosity change with temperature. Meanwhile, the thermal conductivity and specific heat of solid (the load H13 die, the loading tray and the supports) are also defined as function of its temperature. For comparison, simulation was also performed when all the material properties are used as constants under 1050 °C.

Table 1 – Constant used in the k - ε model

C_μ	C_1	C_2	C_3	σ_k	σ_ε	Pr_t
0.09	1.44	1.92	0	1.0	1.3	0.85

4. Results and discussion

The velocity distribution of the gas has been obtained, and is shown through different cross sections (Fig. 3). It can be seen from the panorama that the gas passes through the tubes and nozzles with high velocity and injects into the chamber, and then promptly discharges through the outlet. The gas velocity

near the surface of the die and the corner of chamber is relatively low. Fig. 3a indicates that the velocity of the gas from different nozzles of the same array is unequal, the farther the nozzles locate from the inlet, the higher gas velocity appear. It can be explained that the gas at different positions has different kinetic energy converted from the pressure energy. The gas velocity is sharply decreased when the gas enters the chamber, and it drops to lower than 10 m/s near the surface of the

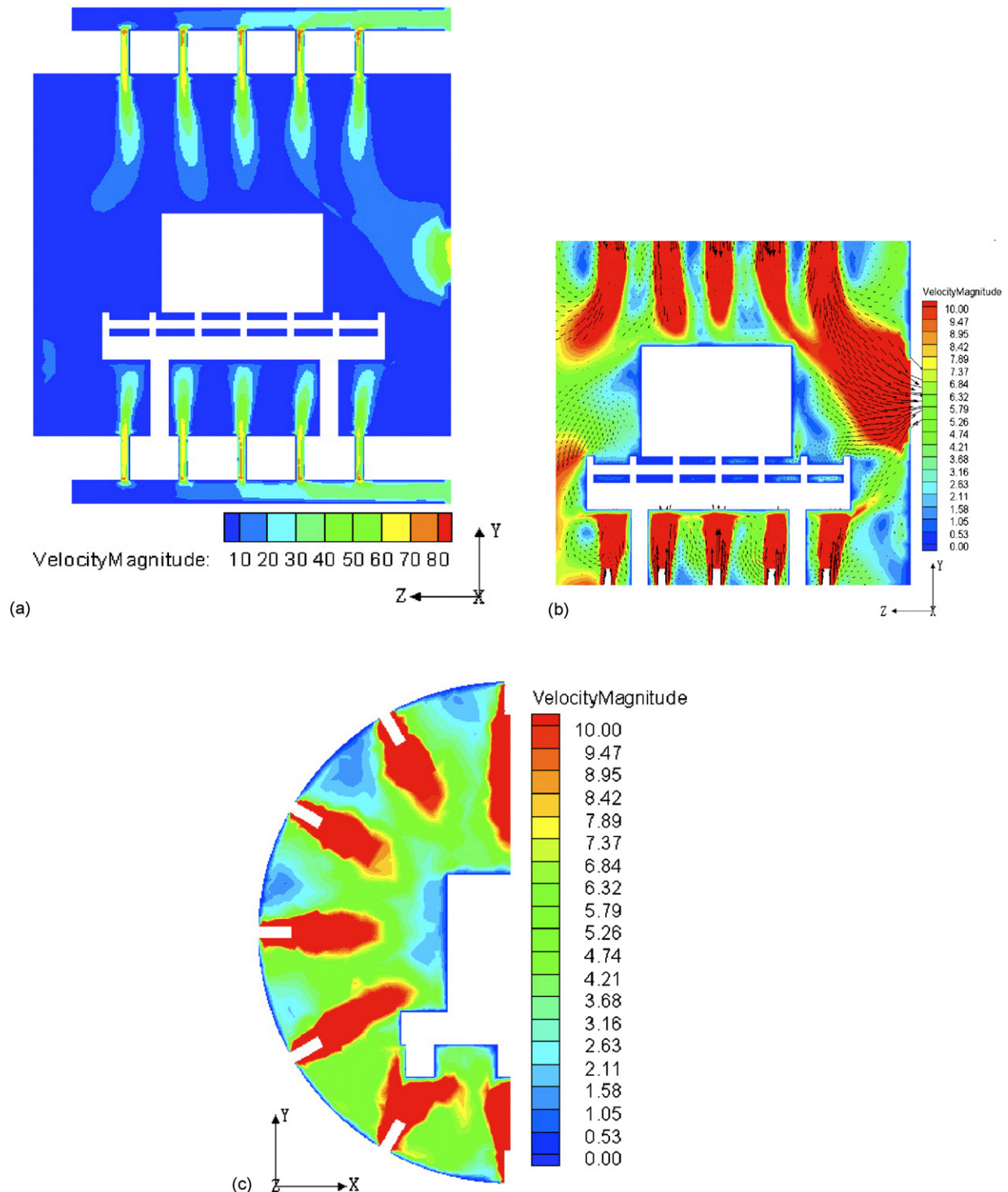


Fig. 3 – Simulation results of velocity distribution at different cross-sections. (a) Velocity contours at the symmetry plane Y-Z; (b) velocity contours and vector at the symmetry plane Y-Z; (c) velocity contours at the cross-section X-Y.

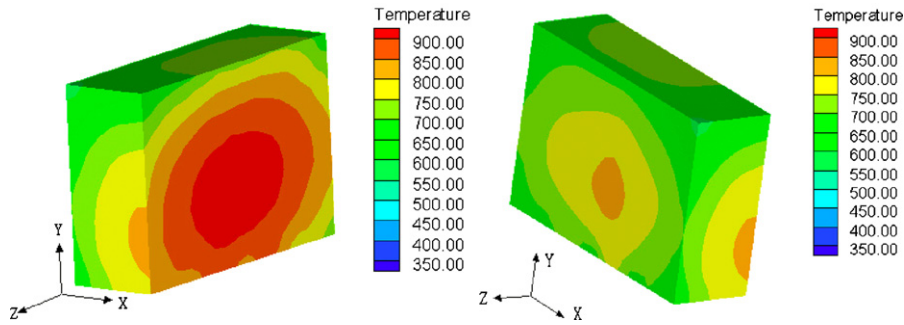


Fig. 4 – Temperature contours inside the die when gas quenched for 128 s.

die with considerable uniformity. In this work, the geometry model thus includes not only the chamber but also the tubes outside the chamber so that the gas inlet velocity can be defined for the whole calculation domain from the tubes. This makes it possible to take into account of the unequal gas velocity from different nozzles, and the simulation results are thus improved. In order to show the details of gas velocity distribution near the surface of the die, the display range of velocity magnitude is adjusted so that the maximum value of gas velocity is 10 m/s (Fig. 3b and c). On each surface, the gas velocity near the corner and edge is usually higher than that near the center. The average gas velocity near the up surface is highest, while that near the bottom surface is lowest, and their difference reaches about 6 m/s, which can be explained that the supports and loading tray obstruct the gas flow. The symmetric gas velocity distribution would be obtained in case the supporting and loading tray were omitted in the geometry model, which deviates from the accurate value.

The gas takes heat flux away from the die, so the gas velocity passing through the surface directly influenced the temperature field inside the die. Fig. 4 shows the simulated temperature contour when the die is quenched for 128 s. The temperature at the center of each surface is higher than that near the corner and edge, and the average temperature of upper surface is higher than that of bottom surface, which is completely corresponding to the gas velocity distribution near the surface of the die. The cooling curves of five monitored points inside the die are extracted from the simulation results, and shown in Fig. 5. The point TC at the center of the load has the lowest cooling rate and the point T1 at the corner has the highest one. The point T4 near the bottom surface has the second lower cooling rate, and the point T2 and T3 have almost the same cooling rate, ranging between that of point T1 and T4. Each point cooling rate basically accords with the measured data as shown in Fig. 6.

The influence of thermal physical properties (such as thermal conductivity, specific heat and viscosity, etc.) has been investigated. Usually, these properties change with the temperature, so they are set as the function of temperature in this work, while the comparing simulation was also conducted with the constant properties of 550 °C. The cooling curves on different points of measured and simulated by two cases are compared in Fig. 7. It can be demonstrated that the errors between two simulation cases are obvious and the simulation results of former case fit the experimental results well.

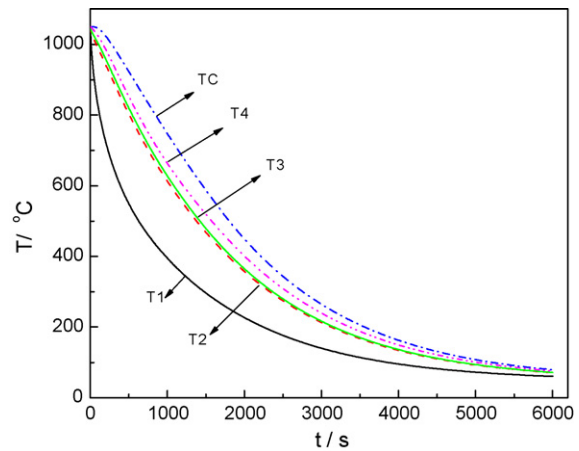


Fig. 5 – The simulated cooling curves at different points in the die using the temperature dependent thermal physical properties of gas and die.

Fig. 7 shows that the experimental and simulated results are in reasonable agreement at the first 2000 s. But in the following slowly cooling down stage, there respectively appear temperature steps on the measured cooling curve of point TC and T2, which is absence in simulated results. This can also be found in Fig. 6 that temperature steps exist on measured cooling curves of T2, T3, T4, and TC, except point T1. The

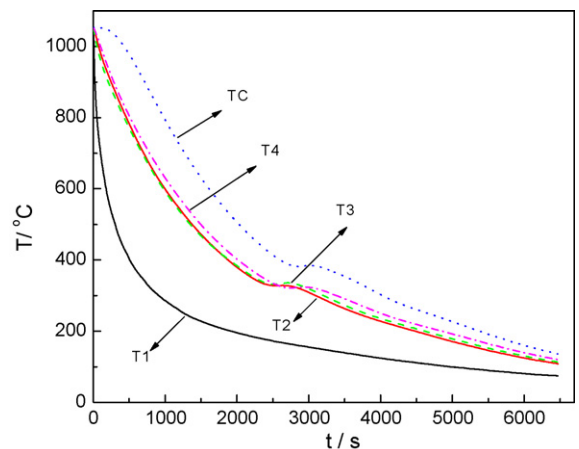


Fig. 6 – The measured cooling curves measured at different points in the die.

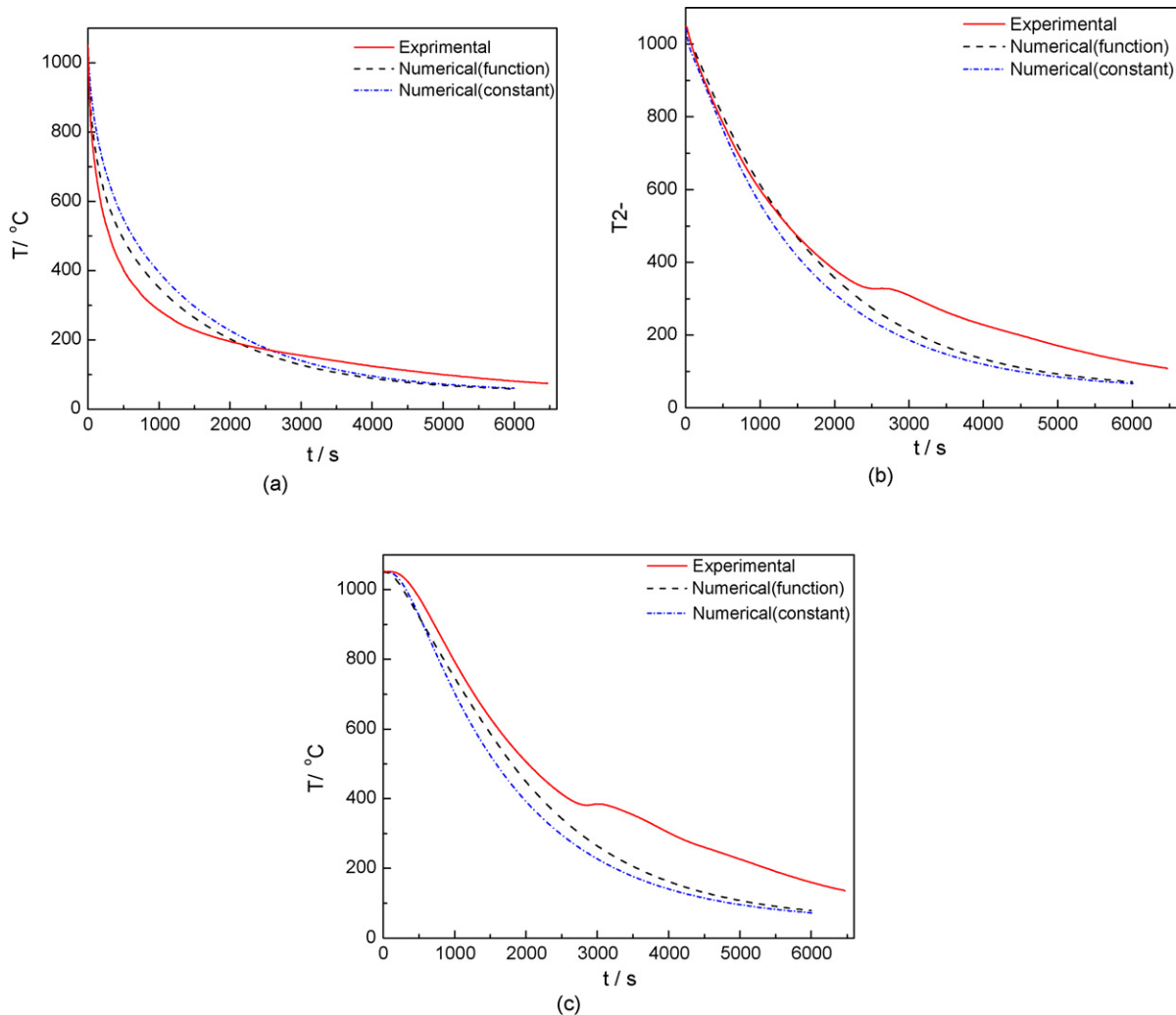


Fig. 7 – Comparison of measured and simulated cooling curves at different points in the die (a) Point T1; (b) point T2; (c) point TC.

steps start at about 380 °C at the point TC and 330 °C at the other points. This may cause by the phase transformation inside the die. According to the CCT diagram of H13 steel, the high temperature austenite decomposes into bainite during this temperature range, which generates heat latent bringing the temperature steps. Because of the high cooling rate, the austenite at point T1 decomposes into martensite instead at about 260 °C (Jeffrey, 1993), and the martensite transformation usually finishes in a very short time. The temperature step cannot be observed on the measured cooling curve of point T1, but it can be observed that cooling rate begins to drop slowly after about 260 °C. Based on the analysis above, the coupled analysis on temperature and flow for gas–solid system can be further improved by considering the phase transformation in the steel.

5. Conclusion

The gas flow filed inside the chamber and the temperature field in the H13 die have been obtained using the computational fluid dynamics package FLUENT, and the simulated and

experimental results are in good agreement. The originality of this work lies on the two facts ensuring the accuracy of simulation results, that, firstly, the geometry model was exactly established according to the set-up of gas quenching chamber, including the load, the loading tray, the supports and other attachments; secondly, the boundary condition of gas inlet velocity was defined at tubes outside the chamber, instead at the nozzles inside the chamber. It is also demonstrated that the thermal physical properties of gas and solid have considerable effect on simulation results, and it is better to set them as the function of temperature, instead of constants under certain temperature. To further improve the accuracy of simulation results, a new complicate model considering the effect of phase transformation inside the load is under development, and related numerical simulation is in progress.

REFERENCES

- Carter, G.C., 1996. Optimizing gas quenching. *Adv. Mater. Process.* 2, 79–82.

- Elkhatatny, I., Morsi, Y., Blicblau, A.S., Das, S., Doyle, E.D., 2003. Numerical analysis and experimental validation of high pressure gas quenching. *Int. J. Therm. Sci.* 42, 417-423.
- FLUENT, User's Guide, United States of America, 2002.
- Jeffrey, A.C., Conybear, 1993. Vacuum hardening of H-13 die steels: experience with convective assisted heating and isothermal holding in regard to distortion and metallurgical properties. *Ind. Heat* 8, 45-48.
- Lubben, T., Hoffmann, F., Mary, P., Laumen, C., 2000. The uniformity of cooling in high-pressure gas quenching. *Heat Treat. Met.* 3, 57-61.
- Lior, N., 2004. The cooling process in gas quenching. *J. Mater. Process. Technol.* 155/156, 1881-1888.
- Pritchard, J.E., Nurnberg, G., Shoukri, M., 1996. Computer modelling of pressure gas quenching in vacuum furnace. *Heat Treat. Met.* 4, 79-83.
- Stratton, P.F., 2002. Modeling gas quenching of a carburised gear. *Heat Treat. Met.* 2, 29-32.